PHYSICAL REVIEW B **91**, 201403(R) (2015)

Spin-dependent size of interband hybridization gap: The interplay of adlayer and substrate states in Pb/Cu(111)

S. N. P. Wissing,[1,*] K. T. Ritter,[1] P. Krüger,[2] A. B. Schmidt,[1] and M. Donath[1]

[1]*Physikalisches Institut, Westfälische Wilhelms-Universität Münster, Wilhelm-Klemm-Straße 10, 48149 Münster, Germany*

[2]*Institut für Festkörpertheorie, Westfälische Wilhelms-Universität Münster, Wilhelm-Klemm-Straße 10, 48149 Münster, Germany*

(Received 11 December 2014; revised manuscript received 21 April 2015; published 8 May 2015)

An interband hybridization gap with spin-dependent size was detected in a low-dimensional electron system influenced by strong spin-orbit coupling. Energy gaps between hybridizing states are distinctly influenced by strong spin-orbit coupling. If the size of these gaps depends on the spin direction of the states, this may lead to fully spin-polarized valleylike structures. As a model system to study the hybridization mechanism behind such valleys, we investigate the unoccupied electronic band structure of Pb/Cu(111) by spin- and angle-resolved inverse photoemission in combination with first-principles calculations. Here, we find a hybridization gap with a splitting of about 200 meV for the one and even larger than 500 meV for the other spin direction. We develop an effective two-band tight-binding model and demonstrate that the interplay of adlayer and substrate states is crucial to induce a sizable spin-orbit coupling and hybridization strength to the interacting states.

DOI: 10.1103/PhysRevB.91.201403 PACS number(s): 73.20.At, 71.70.−d, 79.60.−i

Spin systems of nonmagnetic low-dimensional materials [1,2] are candidates for spintronic applications. Here, the Rashba effect [3], i.e., the spin-orbit coupling (SOC) in combination with broken space-inversion symmetry, lifts the spin degeneracy of the bands [4–6]. One interesting aspect in such two-dimensional electron systems is the influence of the SOC on interacting bands. Bands of parallel or antiparallel spin can hybridize, leading to avoided crossings and hybridization gaps. This has been observed, e.g., for spin-split surface and spin-degenerate quantum-well states on thin Ag films covered with a Bi/Ag(111) surface alloy [7–9] or for two Rashba-split surface states on the surface alloys Bi/Ag(111) [10] and Bi/Cu(111) [11] or thin Pb films on Si(111) [12]. All these systems show a spin-independent hybridization strength and most of them not even an energy gap, but only an avoided crossing. Avoided crossings with spin-dependent hybridization strength were predicted for perovskite oxide interfaces or surfaces [13,14].

An energy gap with a spin-dependent size, however, would lead to fully spin-polarized valleylike structures. Located at the Fermi level (E_F), such valleys could provide a filtering function by suppressing backscattering [15–17], interesting for spin transport properties. For an ultrathin Pb film on Cu(111), we find this type of interband hybridization gap, though located above E_F. Its size differs by more than a factor of 2 for the different spin directions. We choose Pb/Cu(111) [12,18–21] as a model system to investigate the hybridization mechanism behind a spin-dependent gap size. We study it with spin- and angle-resolved inverse photoemission (IPE) [22–24], as well as first-principles calculations. For a qualitative understanding of the hybridization mechanism, we develop a microscopic tight-binding (TB) model. We demonstrate that the interplay of adlayer and substrate states is crucial to induce a sizable SOC and hybridization strength to the interacting states.

Our IPE measurements were performed with spin-polarized electrons [25]. Their spin quantization axis points in the in-plane Rashba polarization direction [6], i.e., perpendicular to their in-plane wave vector $\mathbf{k}_\parallel$ and the surface normal $\mathbf{n}$ [Fig. 1(g)]. The electron beam divergence amounts to $\Delta\theta = \pm 2^\circ$ corresponding to a momentum resolution at E_F and $\overline{\Gamma}$ of $\Delta k_{\parallel,F} = \pm 0.04$ Å^{-1}. The photons are detected with two acetone-filled Geiger-Müller counters with CaF_2 entrance windows. C1 detects photons at a 45° takeoff angle with a mean energy of $\hbar\omega = 9.9$ eV [26]. The heated entrance window of C2 (70° photon takeoff angle) narrows the band pass, thereby shifting the mean detection energy to $\hbar\omega = 9.8$ eV [27]. This improves the total energy resolution of the experiment from $\Delta E = 450$ meV for C1 to $\Delta E = 350$ meV for C2.

One monolayer of Pb atoms was deposited on a pristine Cu(111) substrate by molecular beam epitaxy at a substrate temperature of 575 K. The Pb atoms form a (4×4) reconstructed overlayer, where nine Pb atoms are contracted on the area of 16 Cu atoms, verified with low-energy electron diffraction. The sample was kept at room temperature during the IPE measurements.

Electronic structure calculations were performed using density-functional theory within the local-density approximation (LDA). A basis of Gaussian orbitals is employed together with pseudopotentials including scalar relativistic corrections and SOC [28]. The Pb/Cu(111) surface is treated within a supercell approach using slabs with four Cu substrate layers and a Pb adlayer in a (4×4) unit cell. Relaxations of the topmost four layers were taken into account. The calculated surface corrugation is close to that determined by Müller *et al.* [18]. We simulate the IPE process by assuming a plane wave as the initial state [29,30]. The size of the respective dipole matrix elements $|\langle e^{-i\mathbf{kr}}, \uparrow(\downarrow)|\,\mathbf{Ap}\,|f, \uparrow(\downarrow)\rangle|^2$ is indicated in the plot of the band structure for the final state $|f, \uparrow(\downarrow)\rangle$. $\mathbf{A}$ is averaged over all spatial directions as the polarization of the emitted vacuum-ultraviolet light is not analyzed in the experiment.

Spin-integrated IPE data are presented in Figs. 1(a)–1(c). Five structures are discernible. The feature just above E_F, appearing in Fig. 1(a) at higher negative angles of incidence θ, is interpreted as a Cu(111) surface-umklapp band induced by

*Corresponding author: Sune.Wissing@uni-muenster.de

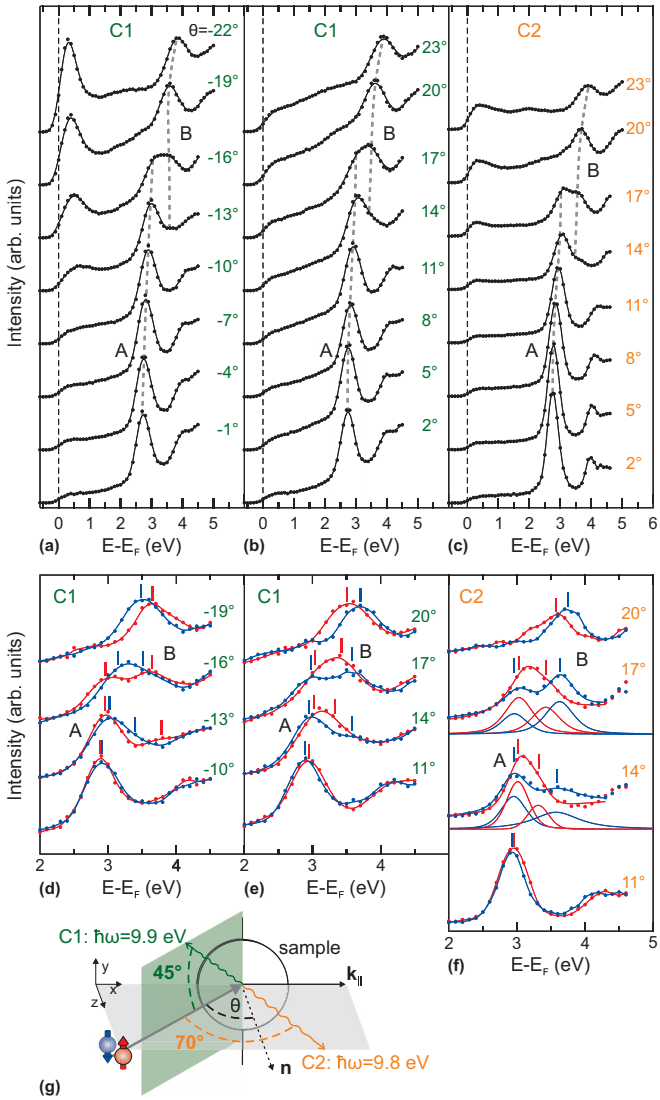

FIG. 1. (Color online) (a)–(c) Spin-integrated and (d)–(f) spin-resolved IPE spectra for various angles of electron incidence θ along $\overline{\Gamma}\,\overline{M}$. Data points represent spin-integrated (black), spin-up (red), and spin-down (blue) intensities. In (f), the peaks extracted from the intensity fits are exemplarily shown for two angles of electron incidence. The series are taken with C1 [(a), (b), (d), (e)] and C2 [(c), (f)] at different photon takeoff angles as sketched in (g).

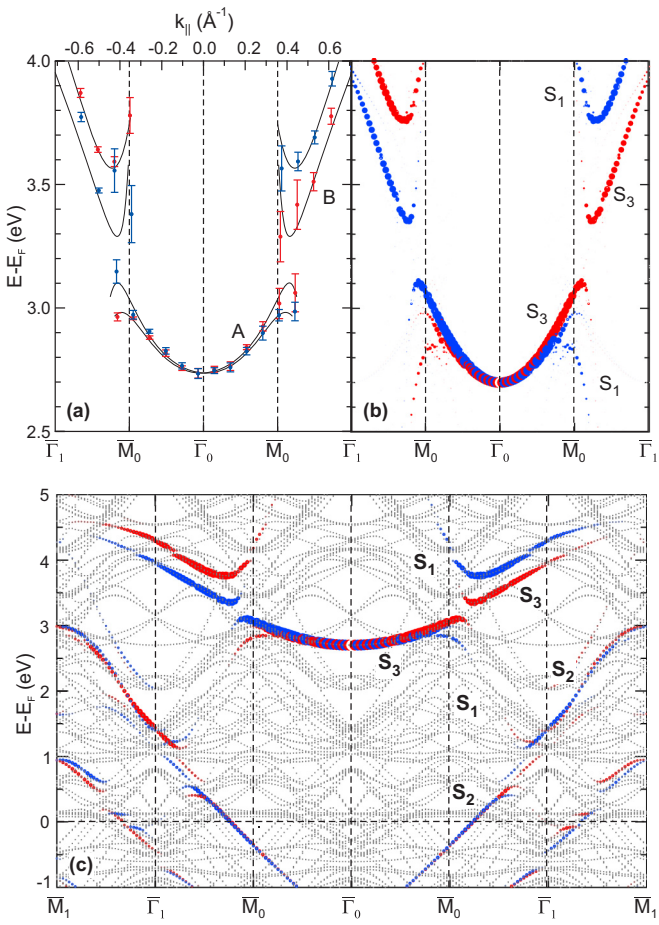

FIG. 2. (Color online) (a) $E(k_\parallel)$ dispersion as derived from the IPE data. The color code is identical to that in Fig. 1. Solid lines, adapted from the calculated dispersion behavior, serve as a guide to the eye. (b), (c) LDA band structure (gray dots) including SOC for the (4×4) reconstructed surface. The degree of polarization in the simulation of the IPE process is indicated in red (blue) where spin-up (spin-down) intensity exceeds. The diameter of the circles is proportional to the absolute square of the dipole transition matrix element (see text) weighted exponentially decreasing with increasing layer depth. (b) Zoom of (c), highlighting the bands where the dipole transition matrix elements exceed 2% of the maximum.

the (4×4) reconstruction. The second structure close to E_F, visible in Fig. 1(c) at higher positive angles, results from a p_z state induced by the Pb adlayer. The image potential state is found at about 4 eV. The two remaining states, labeled A and B, will be discussed in detail below.

At small θ, the spectra are dominated by feature A at 2.6 eV. The significantly higher peak intensity relative to the background in the data of C2 (photon detection angle of 70° compared with 45° for C1) attests to a state with z-dipole emission characteristics. With increasing θ, the intensity of A fades and vanishes for $|\theta| \gtrsim 19°$, while a second feature B appears for $|\theta| \gtrsim 13°$. Spin-resolved IPE data are shown in Figs. 1(d)–1(f) for those θ, where A and B are present in the spectra. Figure 2(a) presents the dispersion $E(k_\parallel)$ deduced from the IPE data with the help of a fitting routine [31], using Voigt profiles on top of a linear background [Fig. 1(f)]. Feature A resembles a Rashba-split band with upward dispersion. For positive $k_\parallel$, the upper branch shows spin-up and the lower branch spin-down polarization and vice versa for negative $k_\parallel$. The spin polarization of B is inverted with respect to that of A.

In Figs. 2(b) and 2(c) the LDA band structure is depicted along $\overline{\Gamma}\,\overline{M}$ within the first two surface-projected Brillouin zones centered around $\overline{\Gamma}_0$ and $\overline{\Gamma}_1$, respectively. The band structure is shifted by $+0.2$ eV with respect to E_F for better agreement with the experimental results.

The inclusion of the IPE process into the calculations demonstrates that the spectral densities do not reflect the periodicity of the (4×4) but of the $(\frac{4}{3} \times \frac{4}{3})$ structure of the Pb adlayer. This is in accord with photoemission results, which reflect the fundamental periodicity of the adlayer and have been interpreted on the basis of the electronic structure calculated for a free-standing Pb layer [19]. Our investigations, however,

show that the coupling of the Pb adlayer to the Cu substrate is essential for the occurrence of spin-dependent hybridization gaps.

Above E_F, we identify a downward dispersing p_x-like state S_1 (with low intensity) and two upward dispersing states, S_2 and S_3, with predominantly p_z character. A Mulliken population analysis [32] shows that their wave functions are mainly located within the Pb adlayer and the first Cu layer. The energy dispersion of S_3 agrees with former experimental findings [20,21]. The band is derived from the Cu(111) surface state, shifted to higher energy by the adlayer and hybridized with a p_z orbital of Pb.

The dispersion and spin texture of the bands [Fig. 2(b)] agree with our experimental findings [Fig. 2(a)]. For small and high $k_\parallel$, i.e., before and beyond the avoided crossing point, A and B are attributed to S_3. The p_z character of S_3 agrees with the observed photon-emission characteristics of A. In the vicinity of the hybridization gap, A and B result from a mixture of the hybridizing bands S_1 and S_3. The hybridization leads to a threefold deviation from two undisturbed crossing bands: (i) The spin splitting is larger beyond the hybridization point. (ii) The sign of the spin splitting changes across the gap. (iii) This results in an apparent step in the dispersion, in particular, for the spin-down branch for positive and spin-up branch for negative $k_\parallel$. In total, this leads to a spin-dependent size of the interband hybridization gap. For positive $k_\parallel$, we find a splitting between the spin-up branches of about 200 meV, while it exceeds 500 meV for the spin-down branches.

For a qualitative understanding of hybridization effects between two spin-split states, a phenomenological interband SOC model was applied in Refs. [10,12]. Starting with the Rashba Hamiltonian [3] for two purely Rashba-split states, a finite interband hybridization term is added to the SOC part of the Hamiltonian. The resulting eigenvalues for two bands are sketched in Fig. 3 for a hybridization of parallel [Fig. 3(b)] and antiparallel [Fig. 3(c)] spin. Both cases do not reproduce the behavior found on Pb/Cu(111) [Fig. 3(a)]. Neither the reversed spin splitting across the hybridization gap nor its spin-dependent size is obtained within this model.

Therefore, we present a microscopic TB model to understand the present hybridization mechanism qualitatively. The model system comprises a Pb(111) monolayer with a p_x and a p_z orbital on top of a Cu(111) monolayer with a p_z orbital per atom. The Pb atoms are located at the hollow sites of the Cu(111) layer to maintain the threefold symmetry of the system. SOC was included in the on-site approximation [33]. The SOC of Cu(111) is very small [34] and, therefore, neglected. For both layers the lattice constant of the compressed Pb layer ($\frac{4}{3}a_{\mathrm{Cu}}$) is used. As the unit cell of the Pb(111)-($\frac{4}{3}\times\frac{4}{3}$) and the Pb/Cu(111)-(4 × 4) have a size ratio of 1:3, the $\overline{M}$ point of the model corresponds to the $\overline{M}_1$ point of the full band structure in Fig. 2(c).

Taking into account the nearest-neighbor contribution for the Pb-Pb, Cu-Cu, and Pb-Cu interaction and choosing the spin-quantization axis in the Rashba direction (the $\pm y$ direction as defined in Fig. 1), the interaction of states with antiparallel spin direction vanishes. For parallel spins, the resulting Hamilton matrices can be written in the basis

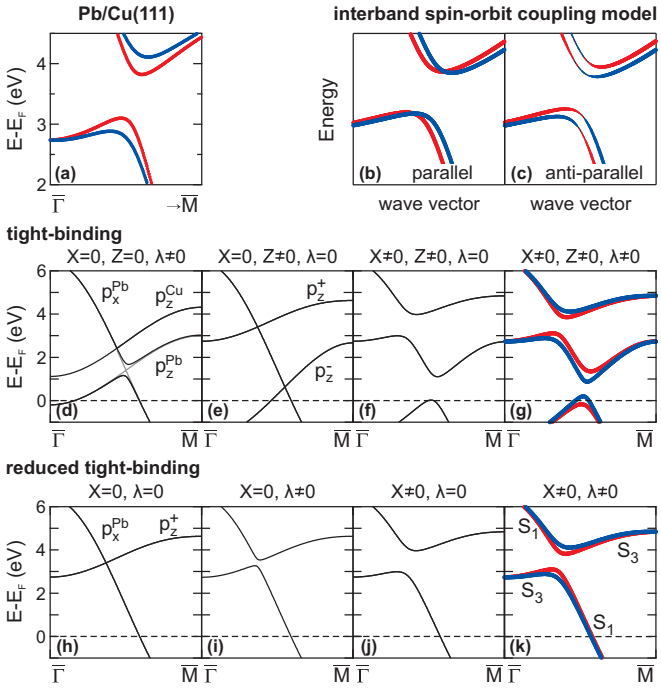

FIG. 3. (Color online) Upper row: (a) Hybridization gap as found on Pb/Cu(111) indicated in red (blue) where spin-up (spin-down) intensity exceeds (black: vanishing polarization). (b), (c) Interband SOC model [10] for hybridization of orbitals with (b) parallel and (c) antiparallel spin. Middle row: TB model including (d) intraband (gray) and spin-orbit (black) interactions, (e) interaction between the p_z orbitals, (f) all interband interactions, and (g) all interband and spin-orbit interactions. Lower row: Reduced TB model including (h) no, (i) spin-orbit, (j) interband, and (k) interband and spin-orbit interactions.

$\{p_x^{\mathrm{Pb}}, p_z^{\mathrm{Pb}}, p_z^{\mathrm{Cu}}\}$ along k_x ($\overline{\Gamma}\,\overline{M}$) as

$$H^{\uparrow} = \begin{pmatrix} H_{xx}^{\mathrm{Pb}} & +i\lambda & X \\ -i\lambda & H_{zz}^{\mathrm{Pb}} & Z \\ X^* & Z^* & H_{zz}^{\mathrm{Cu}} \end{pmatrix}, \quad H^{\downarrow} = \begin{pmatrix} H_{xx}^{\mathrm{Pb}} & -i\lambda & X \\ +i\lambda & H_{zz}^{\mathrm{Pb}} & Z \\ X^* & Z^* & H_{zz}^{\mathrm{Cu}} \end{pmatrix}.$$

All matrix elements depend on TB parameters chosen on the basis of the LDA calculations and, except for the SOC parameter λ, are k dependent. The main diagonal consists of the respective intraband interactions H_{xx}^{Pb}, H_{zz}^{Pb}, and H_{zz}^{Cu}. In the minor diagonal elements we find λ and the interband interaction X (Z) between the p_z^{Cu} and the p_x^{Pb} (p_z^{Pb}) orbitals. No Pb-Pb-interband interaction occurs, as the resulting integrals of the wave functions are zero [35]. The Hamilton matrices for spin up and spin down distinguish themselves by the sign of λ.

Figures 3(d)–3(g) show the eigenvalues of the Hamilton matrices for the different interactions X, Z, and λ. Neglecting interband and SOC, no hybridization occurs [gray line in Fig. 3(d)] between the three spin-degenerate eigenvalues. For $\lambda \neq 0$ (black line) the Cu band is not influenced, whereas a spin-orbit-induced gap opening can be observed between the two Pb orbitals. Without SOC, the interband interaction Z induces a hybridization of the two p_z states [Fig. 3(e)]. Including the interband interaction X, hybridization gaps open

up between the spin-degenerate p_x^{Pb} and $p_z^{\pm}$ states [Fig. 3(f)]. Only if both interband interactions and SOC are considered, the different eigenvalues of $H^{\uparrow}$ and $H^{\downarrow}$ lead to a lifting of the spin degeneracy which results in a spin-dependent gap size as depicted in Fig. 3(g). The hybridization gap between the effective p_z^{+} and the p_x^{Pb} orbital agrees with that found between the states S_1 and S_3.

In the following, we will show that the intrinsic physical characteristics of that gap can even be described by a TB model reduced to the interaction of only two bands. If we consider only the effective p_z^{+} and the p_x^{Pb} orbitals, the resulting (2×2) Hamilton matrices can be written in the new basis $\{p_x^{\mathrm{Pb}}, p_z^{+}\}$ as

$$H^{\uparrow}_{(2\times2)} = \begin{pmatrix} H_{xx} & \frac{1}{\eta}(CX + i\lambda) \\ \frac{1}{\eta}(C^*X^* - i\lambda) & H_{zz} \end{pmatrix},$$

$$H^{\downarrow}_{(2\times2)} = \begin{pmatrix} H_{xx} & \frac{1}{\eta}(CX - i\lambda) \\ \frac{1}{\eta}(C^*X^* + i\lambda) & H_{zz} \end{pmatrix}.$$

Again, the main diagonal consists of the intraband interactions H_{xx} and H_{zz} of the p_x^{Pb} and the effective p_z^{+} orbitals, respectively. On the minor diagonal elements we now find the SOC λ and the interband interaction X between the p_x^{Pb} and p_z^{+} orbital. η and C are renormalization constants resulting from the change to the new basis.

The eigenvalues are depicted in Figs. 3(h)–3(k). Their energetic positions, dispersions, and spin textures agree with those of the full TB model in the respective energy regime above 2 eV. The area around the spin-split p_z^{+}-p_x^{Pb} hybridization gap is enlarged in Fig. 3(a). The main results of the avoided crossing found between the bands S_1 and S_3 are well reproduced: (i) the increase of the spin splitting, (ii) the change of sign of the spin splitting, and (iii) the deviation of the dispersion from that of the undisturbed band. Obviously, the adlayer-substrate interaction is needed to induce a sizable SOC and hybridization strength to the effective p_z^{+} orbital. Most interestingly, the SOC and the Cu-Pb hybridization sum up for spin-down electrons, while they compensate in parts for spin-up electrons. This gives rise to a hybridization gap whose size depends on the spin orientation. To summarize, the heavy element Pb contributes a strong SOC, while the presence of Cu breaks the inversion symmetry and lifts the spin degeneracy of the bands.

In conclusion, we established the presence of interband hybridization gaps with spin-dependent size. Our experimental and theoretical study of the unoccupied electronic structure of Pb/Cu(111) serves as a test case, providing an interband hybridization gap with a splitting of about 200 meV for the one and larger than 500 meV for the other spin direction. With the help of an effective two-band TB model, we demonstrated that the interplay of adlayer and substrate states is crucial to form an effective Pb-Cu state with a sizable SOC and hybridization strength. Hybridization with a Pb state leads to an avoided crossing and a fully spin-polarized valleylike structure. The knowledge of the hybridization mechanism behind such valleys is a cornerstone for the research of nonmagnetic low-dimensional materials where the spin-filtering function of the valley can be used to influence the spin transport properties of the system.

[1] S. Datta and B. Das, Appl. Phys. Lett. **56**, 665 (1990).
[2] I. Žutić, J. Fabian, and S. Das Sarma, Rev. Mod. Phys. **76**, 323 (2004).
[3] Yu. A. Bychkov and E. I. Rashba, JETP Lett. **39**, 78 (1984).
[4] S. LaShell, B. A. McDougall, and E. Jensen, Phys. Rev. Lett. **77**, 3419 (1996).
[5] M. Hoesch, M. Muntwiler, V. N. Petrov, M. Hengsberger, L. Patthey, M. Shi, M. Falub, T. Greber, and J. Osterwalder, Phys. Rev. B **69**, 241401 (2004).
[6] S. N. P. Wissing, C. Eibl, A. Zumbülte, A. B. Schmidt, J. Braun, J. Minár, H. Ebert, and M. Donath, New. J. Phys. **15**, 105001 (2013).
[7] E. Frantzeskakis, S. Pons, H. Mirhosseini, J. Henk, C. R. Ast, and M. Grioni, Phys. Rev. Lett. **101**, 196805 (2008).
[8] K. He, T. Hirahara, T. Okuda, S. Hasegawa, A. Kakizaki, and I. Matsuda, Phys. Rev. Lett. **101**, 107604 (2008).
[9] K. He, Y. Takeichi, M. Ogawa, T. Okuda, P. Moras, D. Topwal, A. Harasawa, T. Hirahara, C. Carbone, A. Kakizaki, and I. Matsuda, Phys. Rev. Lett. **104**, 156805 (2010).
[10] H. Bentmann, S. Abdelouahed, M. Mulazzi, J. Henk, and F. Reinert, Phys. Rev. Lett. **108**, 196801 (2012).
[11] H. Mirhosseini, J. Henk, A. Ernst, S. Ostanin, C.-T. Chiang, P. Yu, A. Winkelmann, and J. Kirschner, Phys. Rev. B **79**, 245428 (2009).
[12] B. Slomski, G. Landolt, S. Muff, F. Meier, J. Osterwalder, and J. H. Dil, New J. Phys. **15**, 125031 (2013).
[13] Z. Zhong, A. Tóth, and K. Held, Phys. Rev. B **87**, 161102 (2013).
[14] P. D. C. King, S. McKeown Walker, A. Tamai, A. de la Torre, T. Eknapakul, B. Buaphet, S.-K. Mo, W. Meevasana, M. S. Bahramy, and F. Baumberger, Nat. Commun. **5**, 3414 (2014).
[15] P. Roushan, J. Seo, C. V. Parker, Y. S. Hor, D. Hsieh, D. Qian, A. Richardella, M. Z. Hasan, R. J. Cava, and A. Yazdani, Nature (London) **460**, 1106 (2009).
[16] H. Hirayama, Y. Aoki, and C. Kato, Phys. Rev. Lett. **107**, 027204 (2011).
[17] K. Sakamoto, T.-H. Kim, T. Kuzumaki, B. Müller, Y. Yamamoto, M. Ohtaka, J. R. Osiecki, K. Miyamoto, Y. Takeichi, A. Harasawa, S. D. Stolwijk, A. B. Schmidt, J. Fujii, R. I. G. Uhrberg, M. Donath, H. W. Yeom, and T. Oda, Nat. Commun. **4**, 2073 (2013).
[18] S. Müller, J. E. Prieto, C. Rath, L. Hammer, R. Miranda, and K. Heinz, J. Phys.: Condens. Matter **13**, 1793 (2001).
[19] F. Baumberger, A. Tamai, M. Muntwiler, T. Greber, and J. Osterwalder, Surf. Sci. **532–535**, 82 (2003).
[20] S. Mathias, A. Ruffing, F. Deicke, M. Wiesenmayer, M. Aeschlimann, and M. Bauer, Phys. Rev. B **81**, 155429 (2010).
[21] S. Jakobs, A. Ruffing, M. Cinchetti, S. Mathias, and M. Aeschlimann, Phys. Rev. B **87**, 235438 (2013).
[22] M. Donath, Surf. Sci. Rep. **20**, 251 (1994).
[23] S. D. Stolwijk, A. B. Schmidt, M. Donath, K. Sakamoto, and P. Krüger, Phys. Rev. Lett. **111**, 176402 (2013).

[24] S. N. P. Wissing, A. B. Schmidt, H. Mirhosseini, J. Henk, C. R. Ast, and M. Donath, Phys. Rev. Lett. **113**, 116402 (2014).
[25] U. Kolac, M. Donath, K. Ertl, H. Liebl, and V. Dose, Rev. Sci. Instrum. **59**, 1933 (1988).
[26] D. Funnemann and H. Merz, J. Phys. E: Sci. Instrum. **19**, 554 (1986).
[27] M. Budke, V. Renken, H. Liebl, G. Rangelov, and M. Donath, Rev. Sci. Instrum. **78**, 083903 (2007).
[28] B. Stärk, P. Krüger, and J. Pollmann, Phys. Rev. B **84**, 195316 (2011).
[29] Please note that an initial state in IPE is equivalent to a final state in photoemission.
[30] A. Damascelli, Z. Hussain, and Z.-X. Shen, Rev. Mod. Phys. **75**, 473 (2003).
[31] S. D. Stolwijk, A. B. Schmidt, and M. Donath, Phys. Rev. B **82**, 201412 (2010).
[32] R. S. Mulliken, J. Chem. Phys. **23**, 1833 (1955).
[33] M. D. Jones and R. C. Albers, Phys. Rev. B **79**, 045107 (2009).
[34] A. Tamai, W. Meevasana, P. D. C. King, C. W. Nicholson, A. de la Torre, E. Rozbicki, and F. Baumberger, Phys. Rev. B **87**, 075113 (2013).
[35] J. C. Slater and G. F. Koster, Phys. Rev. **94**, 1498 (1954).